



ORIGINAL RESEARCH ARTICLE

Mechanical and Metallurgical Properties of Foam Developed by Friction Stir Tube Deposition Technique

Mandeep Kumar, Ratnesh Kumar Raj Singh , and Vivek Jain

Submitted: 27 December 2023 / Revised: 4 July 2024 / Accepted: 14 July 2024

This research seeks to create tube-based aluminum foam using friction stir tube deposition (FSTD) process. In this process, AA6063 consumable rods, pre-filled with a mixture of titanium hydride and aluminum powder, are deposited into a hollow mild steel tube using a conventional vertical milling machine. The results indicate that consumable rods with 12 pre-drilled holes ensure a more uniform distribution of the foaming agent. Furthermore, the study shows that increasing the tool's rotational speed and the weight percentage of titanium hydride results in larger pore sizes and greater porosity. Specifically, for the same TiH₂ composition and rpm levels, the 12-hole filling strategy enhances porosity by 42.62 and 10.12% compared to the 8-hole and 10-hole methods. The optimal process parameters for developing aluminum foam are identified as using consumable rods with 12 holes containing 60% TiH₂ and a rotational speed of 1400 rpm.

Keywords aluminum precursor, foam, frictions stir tube deposition, pore size, porosity

1. Introduction

Advanced steels (Ref 1), light metals such as magnesium and aluminum and their alloys (Ref 2) and cellular structures such as metal foams (Ref 3, 4) and polymer materials are integral to creating lightweight designs. Yet, individual materials alone cannot address challenges related to lightweight materials such as strength, wear resistance, and corrosion. Thus, the use of combination of materials has significantly increased. However, integrating components made from different materials presents a significant challenge and is a key factor in multi-material design. Mechanical and adhesive bonding are the most popular and cost-effective connection methods for development of multi-material system (Ref 5, 6). Another method of sandwiching aluminum foam within aluminum tubes are effectively used to create robust, lightweight components used in automobiles to improve their safety and fuel efficiency (Ref 7). Typically, sandwich tubes filled with aluminum foam are produced by inserting aluminum foam into aluminum tubes (Ref 8-10). Research conducted by Toksoy et al. demonstrates that when foam is bonded to the tubes using adhesives, the sandwich tubes exhibit superior energy absorption capacity (Ref 11). However, these adhesives pose significant environmental challenges by reducing the recyclability of the material.

To overcome this issue, the researchers applied friction stir extrusion (FSE) to as-cast LM13 aluminum alloy, to produce tubes with better microstructural modification and stronger metal bonding between the aluminum tube and foam as reported by Mahyar Talebi et al. (Ref 12). Similarly, Bonaccorsi and co-workers demonstrated in situ development of an aluminum foam-filled steel tube with metal bonding between foam and tube (Ref 13). In this process, aluminum foam is produced using precursor development technique, where a blowing agent powder is evenly distributed in the matrix and placed in the tube which is further heated to induce foam. However, it has been observed that to achieve strong metallic bonding between the foam and the tube, it is essential to either promote the breakdown of the surface oxide or ensure a non-oxidizing environment during the foaming process (Ref 14-16). To overcome this issue, Hangai et al. innovatively coated the inner wall of a metal tube with a foamable precursor using the friction stir-back extrusion (FSBE) technique. Subsequently, they heat-treated the coated tube to produce an aluminum foam-filled metal tube (Ref 17, 18). In this process, the precursor, which is prepared beforehand, is bonded to the metallic tube by FSBE before the heat treatment phase to ensure proper foaming (Ref 19). However, this technique results in an extended lead time due to the sequential placement of the precursor and further processing. So, developing an alternative method to create precursors directly within the tube is crucial and thus, in this study, an innovative approach to fabricate foamable precursor-filled steel tubes is introduced. This technique involves fabrication of precursor by depositing an aluminum rod containing a foamable mixture into the steel tube using the friction stir tube deposition (FSTD) technique. This technique significantly reduces lead time and material wastage during sample extraction. Subsequent heat treatment of the fabricated precursor facilitates foam development. This method not only shortens lead time but also ensures proper particle distribution within the precursor. As this represents a novel approach to foam development, the effect of various process parameters has been investigated rigorously by using Taguchi L18 approach.

Mandeep Kumar, Department of Mechanical Engineering, Chandigarh Engineering College, Chandigarh Group of Colleges, Jhanjeri, Mohali, Punjab 140307, India; and **Ratnesh Kumar Raj Singh** and **Vivek Jain**, Department of Mechanical Engineering, Thapar Institute of Engineering & Technology, Patiala, Punjab, India. Contact e-mail: rkr73@gmail.com.

2. Experimentation

2.1 Materials

In this research, a foamable precursor is developed and further heat-treated for development of aluminum foam. For development of precursor, a mild steel hollow tube with an inner and outer diameter of 26 and 30 mm, respectively, was selected. An aluminum rod of AA6063 alloy with 25 mm diameter and 100 mm in length was selected for deposition. In this rod, the foamable mixtures were filled in the holes that were drilled on the face of rod with a twist drill. A schematic diagram of the consumable rod with drilled holes is shown in Fig. 1(a). The original pictures of the consumable rods after the preparation of holes are shown in Fig. 1(b), (c), and (d). For making a foamable mixture, blowing and stabilizing agents were mixed together in different proportions. The titanium hydrate (TiH_2) was selected as a blowing agent with a mesh size of 325 with 98% purity. The AA6061 powder was selected as a stabilizing agent that has almost same composition as the consumable rod. The purpose of using AA6061 powder is to make a homogeneous mixture of aluminum and titanium hydride during deposition. The titanium hydride and aluminum powders were appropriately mixed in 50-50 (%) and 60-40 (%) weight proportions to form a foamable mixture, as depicted in Table 1. Three different numbers of holes, i.e., 8, 10 and 12, were selected and drilled on the periphery of the consumable rod. The diameter of these holes is selected in such a way that the total area covered by holes is almost constant and thus the amount of foamable mixture is equal for each consumable rod. The positions of holes were selected in such a way that it covers maximum possible surface area during deposition. The other input variables and their range utilized in this experiment are presented in Table 2. These parameters and their range were selected based on prior trial experiment and available machine parameters. The range of parameters that provides defect free precursor in visual inspection was selected. The foamable mixture filling was accomplished in stages to ensure tight filling of the mixture throughout length of the holes without any gap. The ends of the holes are then sealed with an aluminum foil to stop the loose particle of mixture to come out from holes during first engagement of deposition rod to the stud.

2.2 Precursor Development

The precursors were then developed by depositing rotating aluminum rod filled with foamable mixture in the steel tube by friction stir tube deposition process. Figure 2(a) shows the schematics of FSTD process for development of precursor and Fig. 2(b) shows the original foamable mixture filled tube. To insure homogeneous pressing of the foamable mixture during deposition, a 0° tilt of the machine's vertical axis was used. To explore the impact of multiple variables (process parameters) on the quality of developed foam, a thorough experimental design of Taguchi L_{18} orthogonal array is being used for design of experiments. Table 3 displays the set of parameters that have been used in precursor development.

For a clear observation of material deposition in the tube, careful machining has been done of filled tube to reveal the deposited material as shown in Fig. 3(a). This figure clearly shows that deposited material is properly filled in the tube up to its depth. But, it is also observe that, at some locations, defect is also there. These defects were formed due to insufficient

stirring or less plasticity of the depositing material (Ref 20, 21). For a more clear view of material condition during deposition, the cross section at interface of tube and deposited mixture is observed in the optical microscopy. Figure 3(b) shows the interface of mild steel tube and deposited aluminum. It is clearly observed from this image that the aluminum and mild steel are attached together. This is common phenominon in case of processing of aluminum with a steel tool in FSP. This is because during deposition pressure is sufficiently high on the plasticize material to forged it in the steel tube despite of large difference in melting point along with lower solubility of both the materials. For more clear examination and assess the consistency of foamable mixture during deposition, at least three specimens are taken from each tube to carry out mechanical examination for experimental design. The specimens are extracted from the top, middle, and bottom sections of the deposited tube as shown in Fig. 4.

2.3 Heat Treatment

The developed precursor is heat-treated above the decomposition temperature of titanium hydride in an electric furnace to produce foam, as shown in Fig. 5(a). During this process, the samples are kept in a furnace at 670°C for 10 min. As a result, titanium hydride decomposes and releases hydrogen gas. This gas causes the aluminum material to stretch. Since the aluminum matrix becomes soft and semi-solid during heat treatment, it expands. The stretched aluminum matrix traps the hydrogen gas, forming bubbles and leading to the expansion of the sample. The resulting bubbly sample, shown in Fig. 5(c), is referred as foam. The sample is then immediately removed from the furnace and cooled in fresh water at room temperature. Figure 5(d) displays a cross-sectional view of the bubbled structure.

2.4 Sample Extraction

The samples were prepared for testing by cutting them with a precision cutter and smoothing them with emery paper. For metallurgical observations, the samples are first polished with abrasive sheets of various grit sizes and then etched with a modified Keller's reagent. This reagent consists of 5 mL of nitric acid, 3 mL of hydrochloric acid, 2 mL of hydrofluoric acid, and 190 mL of distilled water. After etching, the macrostructure and microstructure of the deposited precursor were observed using optical microscopy. The macrostructural examination of the deposited material reveals the distribution of the foamable mixture. A K-type thermocouple, capable of measuring temperatures up to 800°C , and an Extech (SDL200) data acquisition system are employed to monitor the temperature during the precursor's deposition. The distribution and size of pores in the developed foam are calculated using "Image J" software.

3. Results and Discussion

3.1 Macrostructure

The macrostructure of the deposited precursors was examined to assess the overall behavior of material flow in the deposited region. Most macrographs exhibited an onion-ring pattern of material flow, clearly visible in the deposited zone

(DZ) through optical microscopy, as shown in Fig. 6(a), (b), (c), (d), (e), (f), (g), (h), and (i). The results indicate that significant stirring occurred during deposition, causing the material to undergo dynamic recrystallization. This stirring ensured the proper distribution of the foaming mixture within the deposited material. However, in some areas of the deposited samples, clusters of mixtures were observed. These clusters were particularly prevalent in cases with fewer holes and lower speeds, likely due to insufficient stirring during precursor development.

Figure 6(a), (b), and (c) illustrates the macrostructure of the deposition zone with an 8-hole profile rod at various speeds. The clustering of foaming agent particles is clearly visible at all rotational speeds, with fewer particles in certain locations. This occurs because the 8-hole profile covers a smaller area for mixture distribution, resulting in a limited quantity of mixture particles in localized regions. However, as the speed of the rotating rod increases from 900 to 1400 rpm, the clustering of the mixture decreases, as shown in Fig. 6(b) and (c). Additionally, increasing the number of holes from 8 to 10 in the consumable rod significantly enhances the dispersion of the mixture, covering a larger distribution area during deposition, as illustrated in Fig. 6(d), (e), and (f).

The 10-hole rod demonstrates superior performance compared to the 8-hole rod at all rotational speeds. However, clustering of foaming particles is observed at a lower speed (800 rpm), as depicted in Fig. 6(d). This observation suggests

that at lower speeds, the matrix material solidifies rapidly, causing the distribution of foaming particles to become fixed in specific positions, resulting in particle clustering. On the other hand, the 12-hole rod achieves a more homogeneous mixture compared to lower-hole profile rods, as illustrated in Fig. 6(g), (h), and (i). A more uniform distribution ensures the formation of more spherical pores. Due to this homogeneous mixing of foaming agents, the 10-hole and 12-hole rod profiles are expected to deliver more consistent results, as evidenced by the microstructure of the deposited samples. At high temperatures, the material undergoes significant plastic deformation, leading to the creation of refined, near-equivalent-shaped recrystallized grains.

3.2 Microstructure

The microstructure of the deposited material was thoroughly examined at various locations from top to bottom. Figure 7(a) presents a cross-sectional view of the deposited tube sample,

Table 1 Powder composition

Sr. No.	Composition, wt.%	Notation
1	TiH ₂ (50%) + Al 6061(50%)	A
2	TiH ₂ (60%) + Al 6061(40%)	B

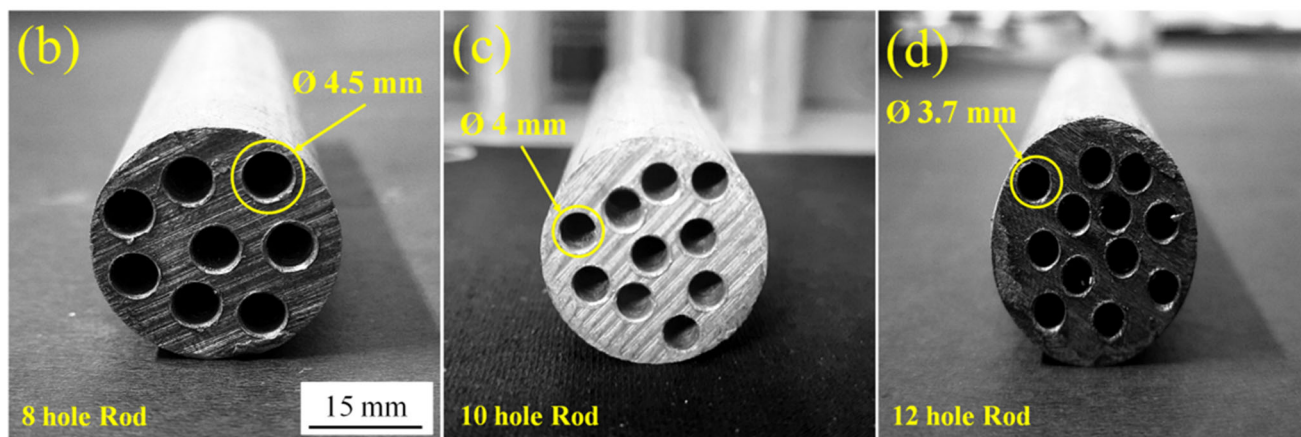
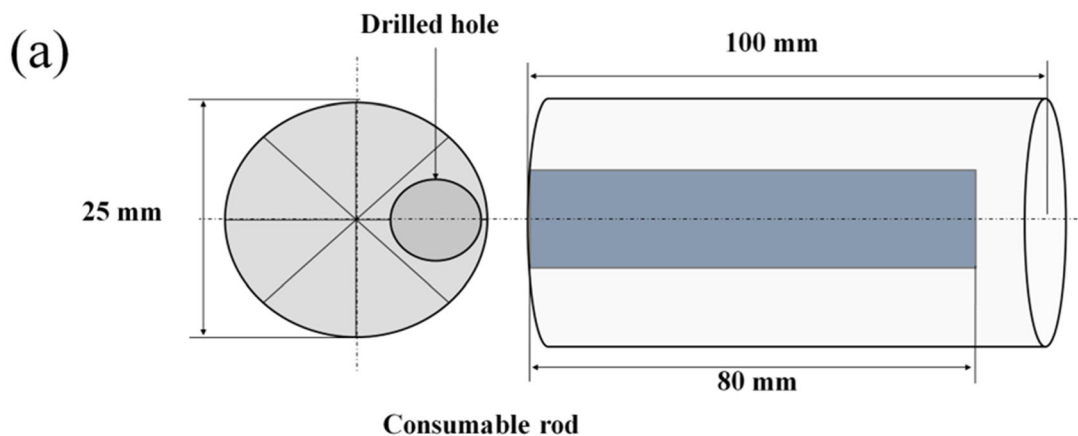


Fig. 1 (a) Schematic diagram of the consumable rod, (b-d) Original images of the rod after drill

highlighting the areas where microstructural examinations were performed. The microstructure at the top zone of the deposited material, depicted in Fig. 7(b), reveals low segregation of the foaming mixture along with minimal material flow patterns. In this zone, a recrystallized grain structure is evident, showing a mix of grains varying in size.

Figure 7(c) illustrates the material flow pattern in the middle region of the deposited sample. A thermocouple, discussed in the next section, is attached at this location to measure the temperature, which ranges from 450-510 °C during deposition. This temperature is sufficient to promote post-deposition grain growth, resulting in larger grains compared to those reported in the friction stir-deposited zone in the published literature (Ref 22). As Fig. 7(d) shows, clustering of the foamable mixture is observed at the bottom of the sample, which may be due to insufficient plastic deformation of the material at the initial point of contact.

The distribution of the mixture is also affected by the rpm of the rotating rod. As rpm increases, a uniform distribution of foamable mixture increases, which may happen because the severity of deformation increases with increasing rpm during deposition. This phenomenon is observed in Fig. 8(a), which shows the clustering of the mixture at some locations in deposited samples at a lower rotation speed of 900 rpm. As the rotation speed increases from 900 to 1120 rpm, the clustering of foamable particles decreases, as shown in Fig. 8(b). The clustering of these particles further decreases with an increase in rpm from 1120 to 1400 rpm (Fig. 8c).

The SEM analysis of deposited material was also been conducted to see the distribution of particles and changes in microstructure in the deposited material. Figure 9 shows the SEM images of the deposited material. Figure 9(a) shows the

Table 2 Factors and their levels

S. No.	Factors	Levels	L1	L2	L3
1	Composition, wt.%	2	A	B	
2	Number of holes	3	8	10	12
3	Rotational speed, rpm	3	900	1120	1400

clustering of foaming mixtures in the deposited material. This clustering is observed in a random pattern in the deposited material, possibly due to the deformation of material and plastic flow during deposition. The fine grain structure is also observed in the deposited zone (Fig. 9b), which shows recrystallization due to the plastic deformation of the material during deposition.

3.3 Temperature Profile

The rise in temperature during the deposition process was also recorded during the experiments. This rise in temperature in the deposition zone (DZ) results from friction and plastic deformation. This temperature causes the plastically deformed deposition rod to attach to the stud at the tube's end. Then layer by layer, deformation and bonding occur until the whole rod is deposited into the tube. A K-type thermocouple is employed to monitor the temperature of the deposition zone, as shown in Fig. 10. Figure 11(a), (b), (c), (d), (e), (f), (g), (h), and (i) illustrates the recorded temperature at the midpoint of the tube

Table 3 Experimental design

Sr. No.	Composition	Number of holes	Rotational speed, rpm
1	A	8	900
2	A	8	1120
3	A	8	1400
4	A	10	900
5	A	10	1120
6	A	10	1400
7	A	12	900
8	A	12	1120
9	A	12	1400
10	B	8	900
11	B	8	1120
12	B	8	1400
13	B	10	900
14	B	10	1120
15	B	10	1400
16	B	12	900
17	B	12	1120
18	B	12	1400

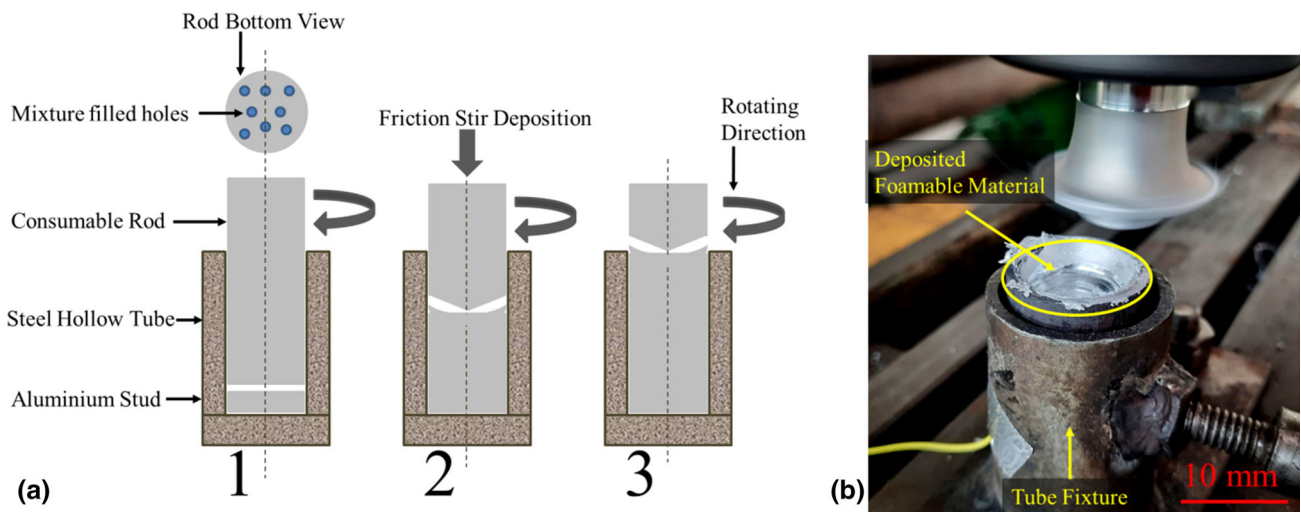


Fig. 2 Consumable rod deposition (a) Sectional view and (b) Original deposited material tube

for various rpm and hole numbers. A heating curve is shown by the graph's upward slope, and a cooling curve is indicated by the graph's downward slope. The frictional heat produced between the rod and substrate is used to compute the temperature history of the deposition process. Even though all rod profiles cover the same area for deposition during stirring, the material's plastic deformation varied because of the number of holes and stirring speed. The temperature generated is 444.6 °C at 800 rpm, while it is 513 °C and 469.2 °C at 1400 and 1120 rpm, respectively, during the friction stir tube deposition process, as illustrated in Fig. 11(a), (b), and (c). Similarly, the 10- and 12-hole profiles also achieved temperatures in the 450 to 513 °C range at different rotating speeds, just like the 8-hole rod. The temperature ranges between these friction stir tube deposition samples are very similar but the highest temperature is recorded at 1400 rpm which is 513 °C as shown in Fig. 11(i). This means that at higher speeds, the severity of plastic deformation increases during deposition (Ref 23, 24). This phenomenon is observed in all samples irrespective of number of holes. Thus, it is clear that the increasing number of holes in the rod does not influence heat generation during the friction stir tube deposition process, and only speed is the influencing parameter for temperature.

3.4 Developed Foam

The precursor developed by this technique is further heat-treated in a furnace for the development of foam. Figure 12(a), (b), (c), (d), (e), (f), (g), (h), and (i) displays foam samples produced with various drilled holes and rotating speeds (rpm). The scan images indicate the location of the pores on the foam sample's surface. A developed foam sample that has been deposited by an 8-hole rod at various speeds is shown in Fig. 12(a), (b), and (c). A bigger hole in the developed foam is observed in Fig. 12(a) and highlighted by a red circle, indicating the foaming mixture clustered at a particular location on a lower speed level. This occurs because, during stirring, the foamable mixture is deposited in large quantities at particular locations and is not spared adequately in the deposition zone. The clustering decreases as the rotating speed rises, as illustrated in Fig. 12(b) and (c). This may be due to more stirring and increased frictional heat, maintaining the proper

distribution of material and adequate temperature in the deposited zone promotes smooth stirring of material (Ref 23). As demonstrated in Fig. 12(d), (e), and (f), better results in material distribution are obtained by increasing the number of holes in the rod from 8 to 10. However, clustering of the mixture was also observed in scan images taken at a lower rpm, similar to the 8-hole rod configuration as shown in Fig. 12(d). The 10-hole rod produces a homogeneous mixture at greater speeds (1120 and 1400 rpm) in comparison to lower speeds. It has a more uniform distribution of foaming material and less particle clustering compared to 8-hole rod since it covers a broader area for distribution (Ref 23). The pores are also evenly distributed throughout the foam samples and cover a large surface area. Similar to this, the results at the 12-hole rod are better since less particle clustering is seen at lower speeds, as seen in Fig. 12(g). The reason for this is that a rod with 12 holes has a larger distribution area than one with 8 or 10 holes. Similarly, at greater speed levels, a finer and uniform distribution of the mixture is obtained, as seen in Fig. 12(h) and (i). Defects in the developed foam started to appear when more than 12 holes were drilled in the consumable rod because the

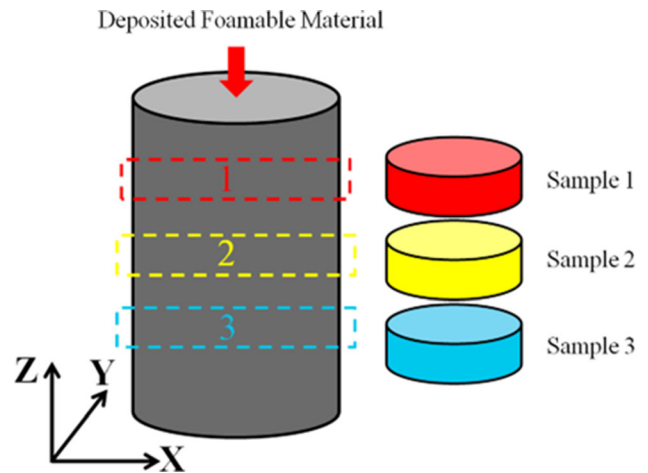


Fig. 4 Extraction of the samples

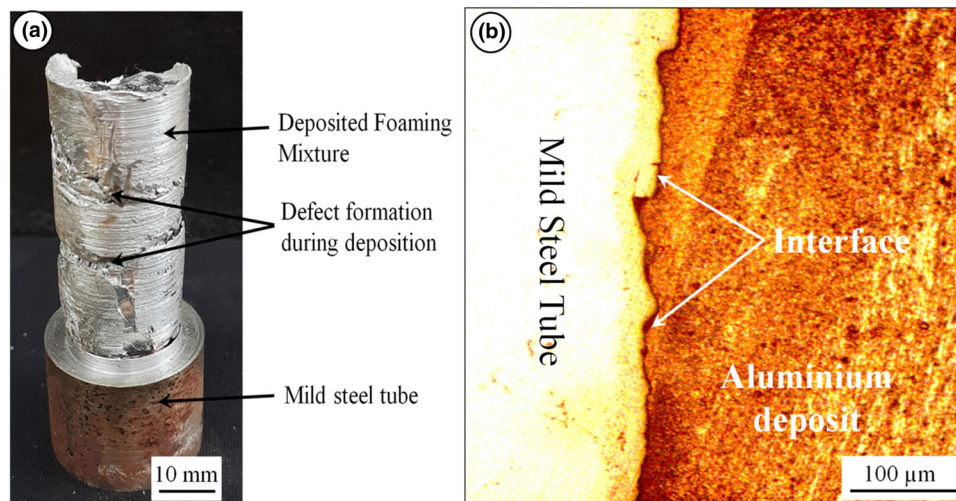


Fig. 3 (a) Deposited materials with defects (b) interface of deposited material and mild steel tube

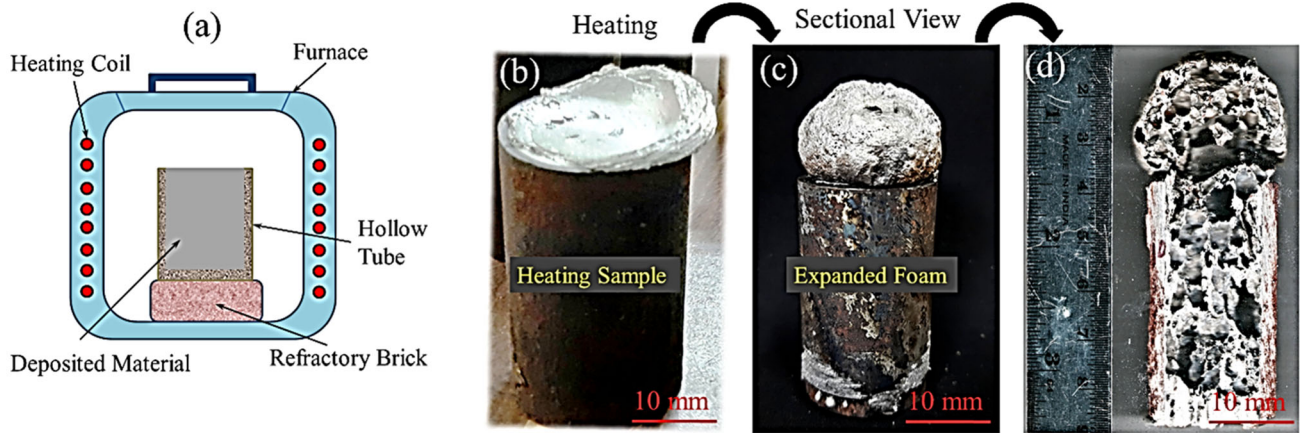


Fig. 5 (a) Schematic diagram of sample heating in furnace, (b) expanded foam sample and (c) expanded foam sectional view

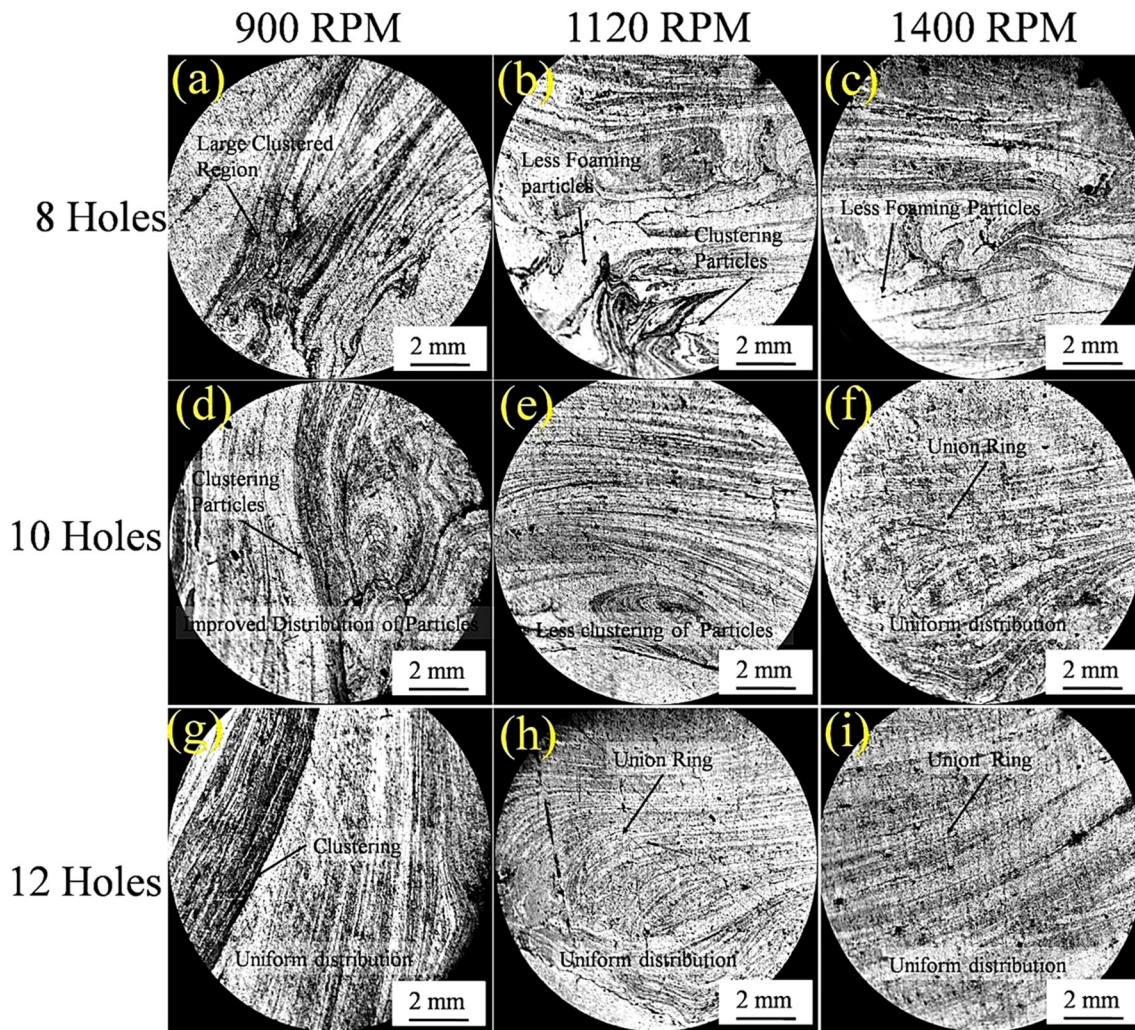


Fig. 6 Material flow pattern for 8-hole profile rods at (a) @ 900 rpm (b) @ 1120 rpm and (c) @ 1400 rpm, 10-hole profile rod at (d) @ 900 rpm, (e) @ 1120 rpm and (f) 1400 rpm and 12-hole profile rod at (g) @ 900, (h) @ 1120 rpm and (i) @ 1400 rpm during friction stir tube deposition process

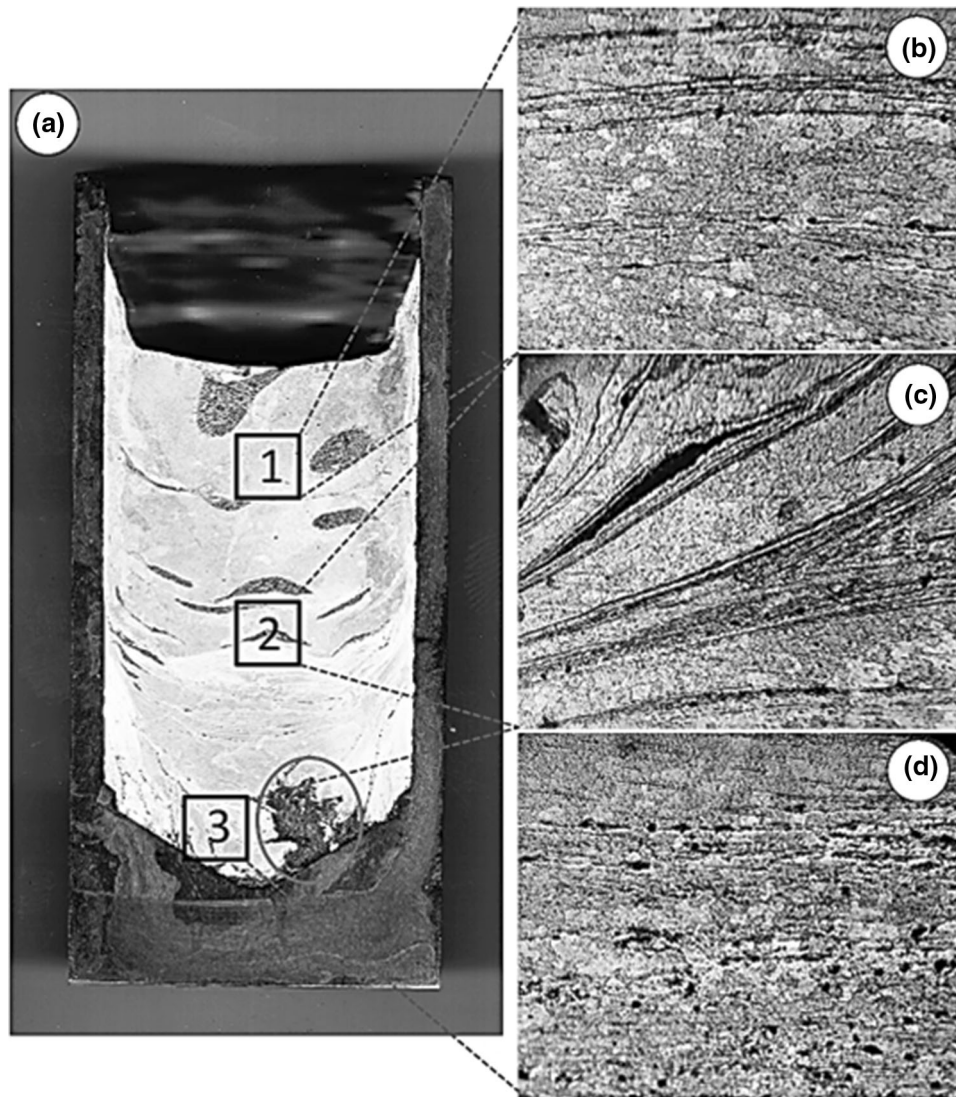


Fig. 7 (a) Deposited precursor sectioned view and Microstructure at (b) top, (c) middle and (d) bottom zone position

rod had a greater amount of the foamable mixture than the matrix. This causes small pores to merge to form large pores, reducing the foam quality.

3.5 Pore Development

Pore development is examined by the composition of the powder and the number of holes. The average pore size falls as the number of holes on the rod's perimeter increases. The pore size is 3.93 mm at a 60% composition of the blowing agent and 2.85 mm at a 50% composition. The cross section of foam developed with an 8-hole profile with varying blowing agent content is shown in Fig. 13(a). The findings show considerably more particle clustering and very little blowing dispersion in the 8-hole profile rod. This is because the foaming particles in an 8-hole profile cover less surface area during deposition, which leads to incorrect blowing agent distribution and the production of large holes after heating. Due to the reduced amount of foaming agent in the mixture at 50% composition, pore size decreases. As the number of holes in the rod increases from 8 to 10, as shown in Fig. 13(b), there are some improvements in pore size observed in the developed foam.

This is due to the uniform mixing of powders at more holes in the rod, which covers more area for the distribution of blowing agent and less clustering of the particles as compared to the 8-hole profile. The average pore size at 60% and 1.56 mm at 50% composition of TiH₂. A similar type of result is also seen in the 12-hole profile rod, as shown in Fig. 13(c). By increasing the number of holes from 10 to 12, a more uniform mixing of the blowing agent is obtained which reduces the size of pores. In comparison to 8 and 10-hole profiles, the pore size in the 12-hole profile is 1.57 mm at 60% and 1.49 mm at 50% of titanium hydride composition.

The pore distribution was measured based on the composition, number of holes, and rotation speed (rpm). The pore size results presented here are the average values of three samples taken from different locations of the foamed sample. It was found that pore size increases with the weight percentage of titanium hydride. The results also reveal that the 12-hole consumable rod, across all compositions, produces a smaller pore size compared to other hole configurations. Increasing the tool's rotational speed, results in smaller pore diameters for both compositions, as clearly illustrated in Fig. 14(a). The

interaction graph in Fig. 14(b) shows that, pore size decreases continuously as the number of holes increases, regardless of varying composition and rotating speed. This is because a greater number of holes allow the foamable mixture to be

deposited over a larger area during deposition, leading to a more uniform distribution of titanium hydride particles. A similar pattern is observed with rotational speed (rpm) concerning composition and the number of holes, as evident in



Fig. 8 Microstructure at (a) 800 rpm, (b) 1120 rpm and (c) 1400 rpm

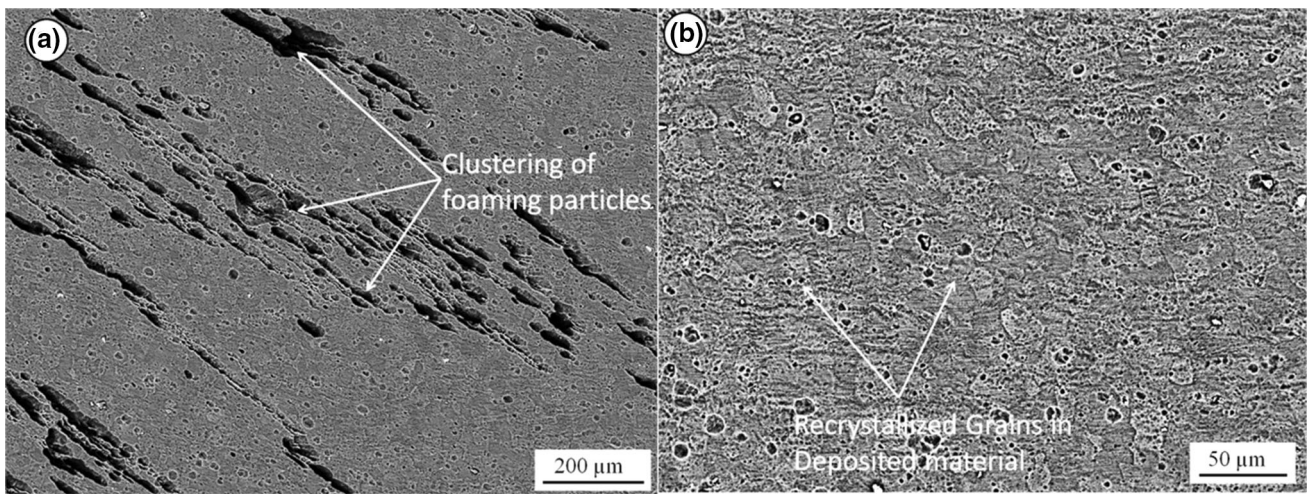


Fig. 9 SEM images (a) clustering of foaming mixture (b) recrystallized grains in deposited material

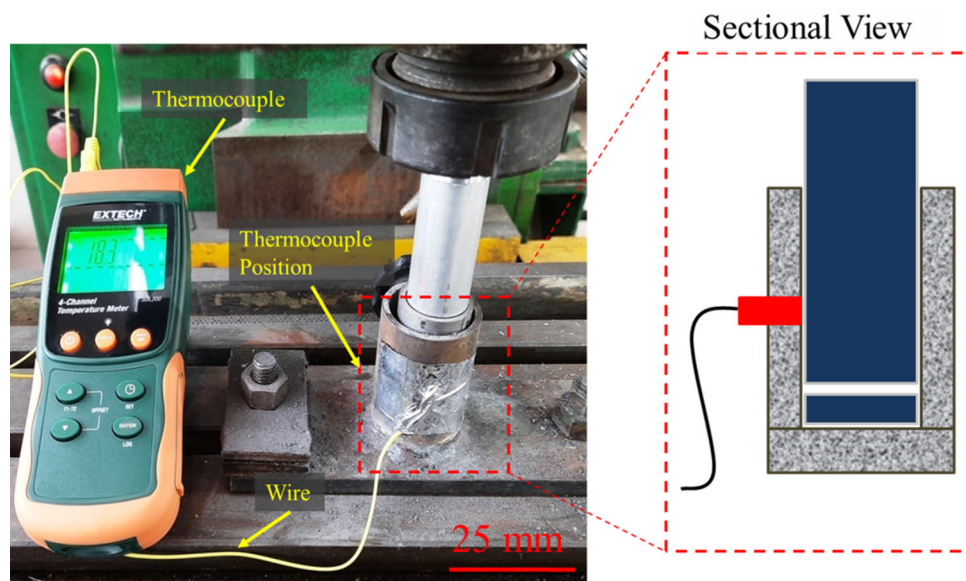


Fig. 10 Thermocouple machine setup and sectional view

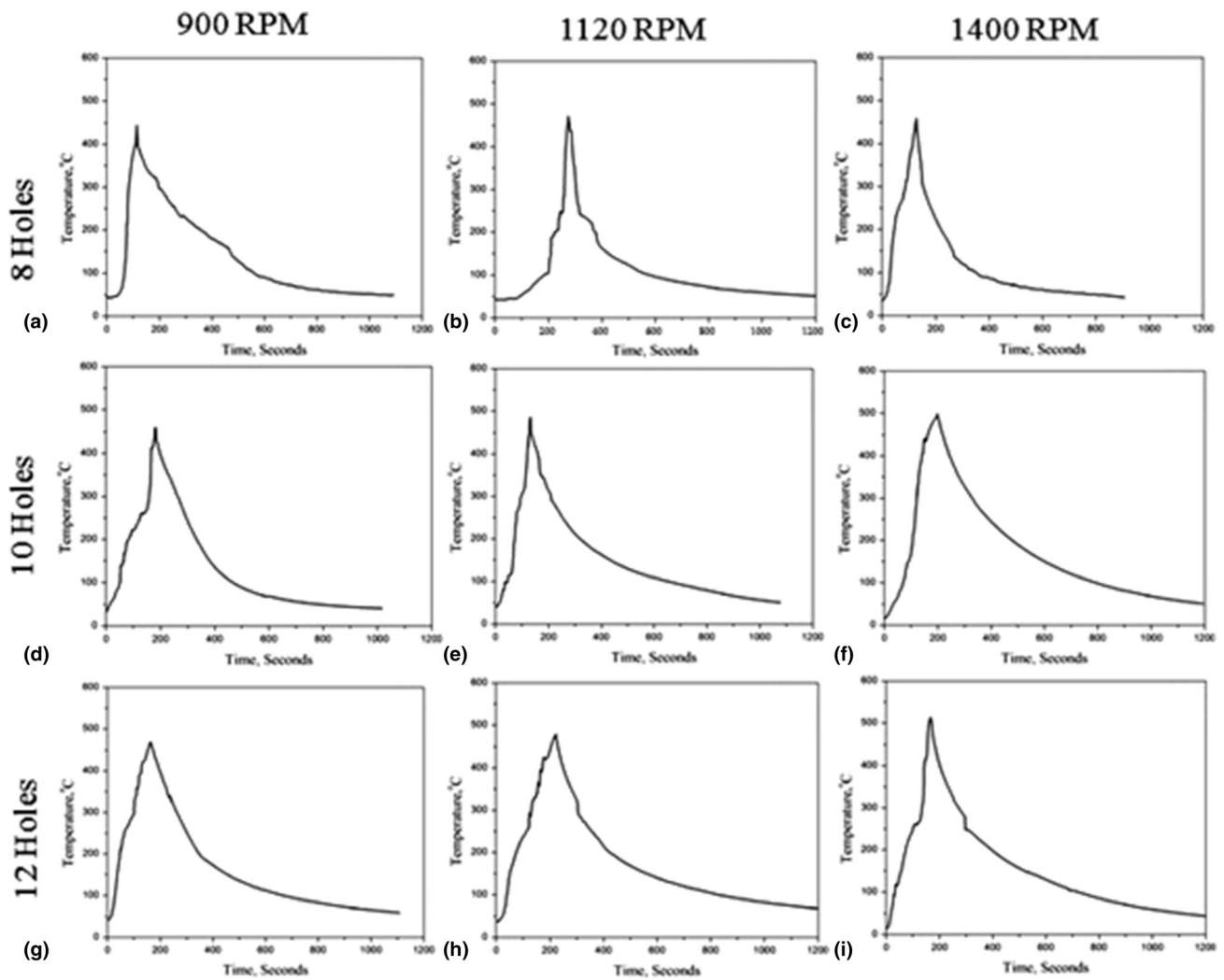


Fig. 11 Temperature generation during friction stir tube deposition process for 8-hole profile rod at (a) @ 900 rpm, (b) @ 1120 rpm and (c) @ 1400 rpm, 10-hole profile rod at (d) @ 900 rpm, (e) @ 1120 rpm and (f) @ 1400 rpm and 12-hole profile rods at (g) @ 900 rpm (h) 1120 rpm and (i) 1400 rpm

Fig. 14(c). This is due to the material being continually deformed at higher speeds, which enables the foaming powder to mix more thoroughly and evenly into the matrix.

The variation in porosity is illustrated in Fig. 15(a), (b), and (c), which consider composition, number of holes, and rotation speed as variable factors. The number of holes and the rotating speed (rpm), both connected to composition, impact the foam's porosity, as shown in Fig. 15(a). The results indicate that the developed foam becomes more porous as the rotational speed and the number of holes increase. Additionally, composition "B" exhibits a higher porosity percentage than composition "A." The 12-hole consumable rod provides greater porosity than the 8- and 10-hole configurations in all scenarios, as depicted in Fig. 15(b). Figure 15(c) shows similar outcomes, where increasing rotational speed leads to increased porosity due to enhanced stirring in the deposited zone, resulting in a homogeneous distribution of foaming agents throughout the structure.

The results reveal that higher TiH₂ composition and rpm result in improved porosity. At 1400 rpm, the 12-hole filling technique achieves a maximum porosity of 87%, while the 8- and 10-hole filling techniques reach porosity levels of 79 and

61%, respectively. This demonstrates that foam with a higher porosity percentage, specifically using the 12-hole technique, contains a greater percentage of pores due to the uniform distribution of foaming agents throughout the structure.

3.6 Compression Test

Compression tests were conducted to evaluate the compressive behavior and energy absorption capacity of foams. Several variables, including pore size, porosity, alloy composition, and the composition of the foaming agent within the foam structure, significantly impact the compression behavior of aluminum foams (Ref 25). To analyze the effects of these different parameters on foam developed by the friction stir tube deposition technique, samples produced under various conditions were selected for the compression test. To determine the force absorption capacity in different directions, samples with approximately 50% porosity were tested in two separate orientations at a constant strain rate of 1 mm/sec. Figure 16 illustrates the deformation pattern of the sample during the compression test in a flat position (in the XY plane, as depicted in Fig. 3). The stress-strain curves of the samples, along with

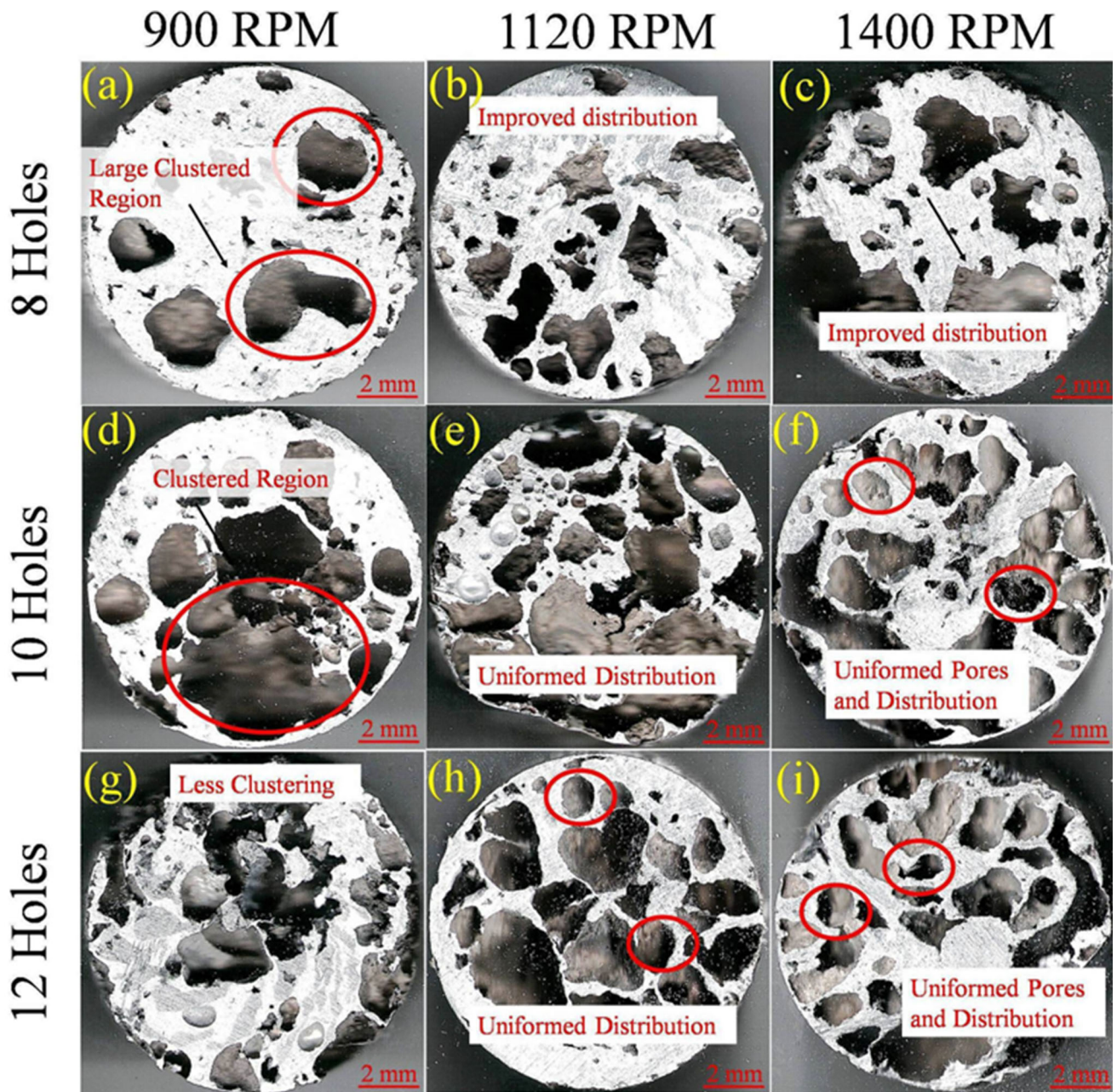


Fig. 12 Developed foam samples at various rotating speed for 8-hole profile rod at (a) @ 900 rpm, (b) @ 1120 rpm and (c) @ 1400 rpm, 10-hole profile rod at (d) @ 900 rpm (e) @ 1120 rpm and (f) @ 1400 rpm and 12-hole profile rod at (g) @ 900 rpm, (h) @ 1120 rpm and (i) @ 1400 rpm

their deformation at various stages from 0 to 80%, are shown in Fig. 16(a), (b), (c), (d), and (e) under the flat position. The compression test images display three phases of deformation (Ref 26). Initially, due to the preliminary stress that the structure must withstand, deformation begins slowly. In this first stage, stress increases with strain due to the initial strength of the foam.

Afterward, the foam begins to deform more significantly with only a minor increase in stress. This happens because the stress exceeds the capacity of the foam cell walls, causing them to deform. This stage is known as the second stage or constant deformation zone, where strain increases with little corresponding increase in stress. Figure 16(b) and (c) illustrates this

second phase of the compression tests. As shown in the stress-strain graph in Fig. 16(e), the second region displays a steady deformation range, referred to as the plateau zone. This plateau stress is crucial for characterizing the foam's energy absorption behavior and is an essential factor in the foam's compression performance. After 65 to 70 percent deformation, the third phase of densification begins, marked by a rise in stress with increasing strain. Figure 17(a), (b), and (c) depicts the compression behavior of samples created with 8, 10, and 12 holes, respectively. The findings indicate that as the number of holes in the consumable rod increases, the porosity raises, causing the sample's plateau range to extend.

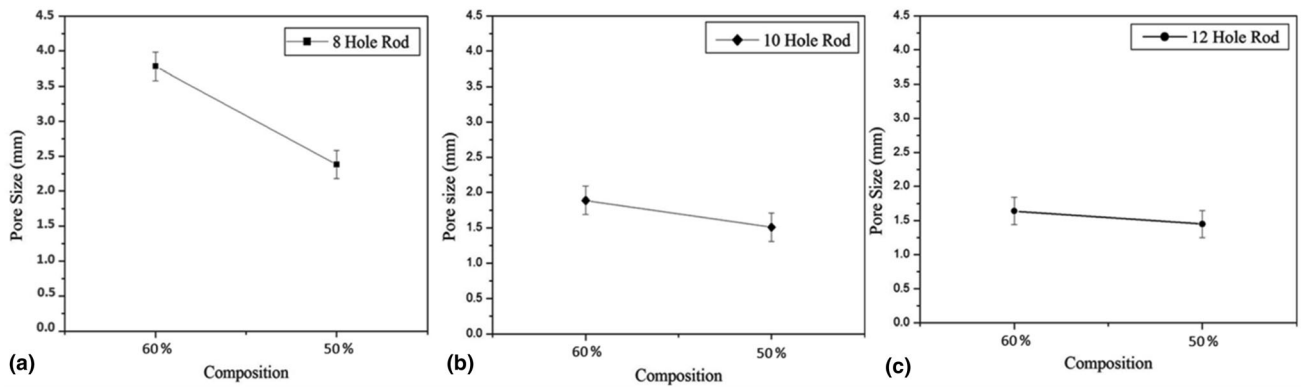


Fig. 13 Titanium hydride composition effect on pore size (a) 8-hole, (b) 10-hole, (c) 12-hole profile rods at 50 and 60% Composition

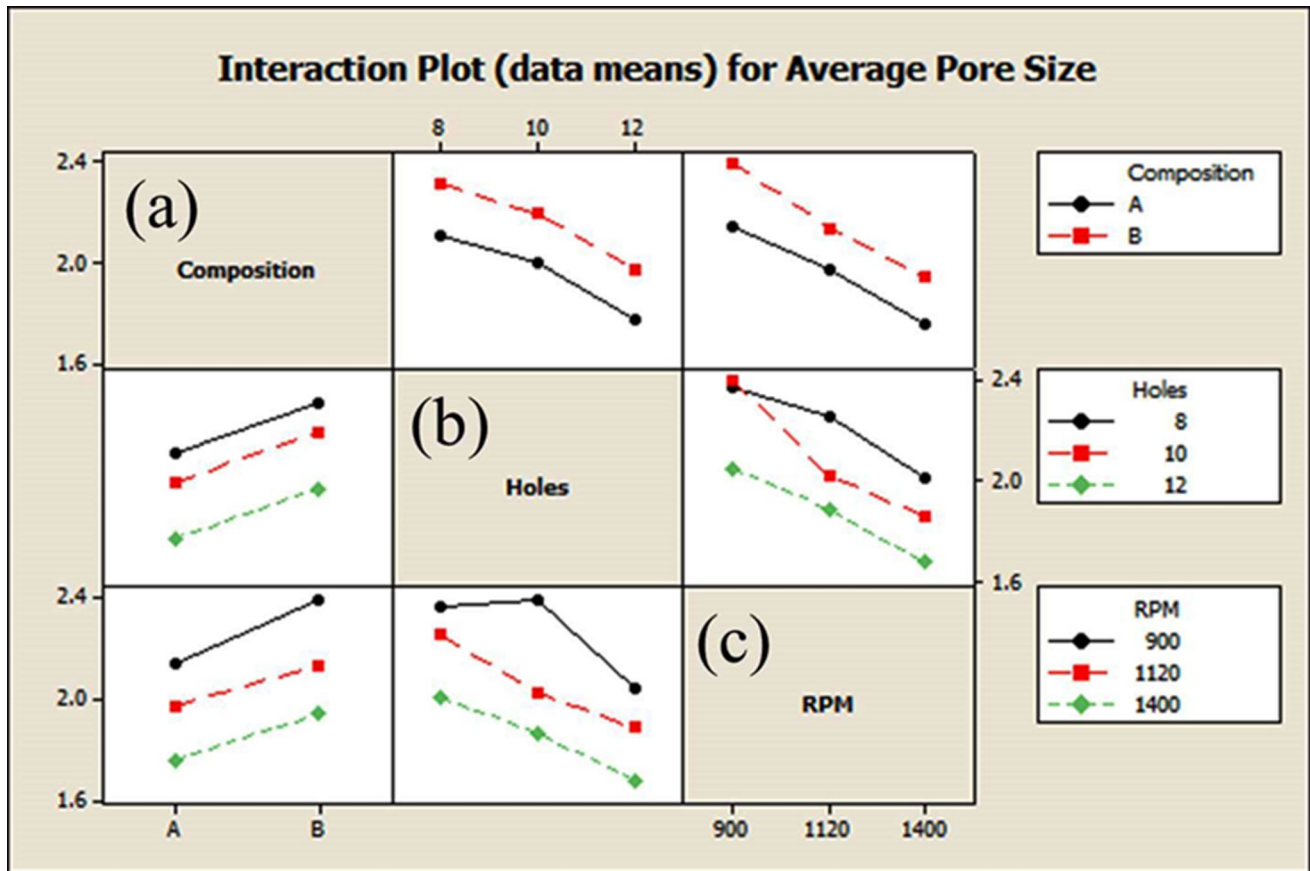


Fig. 14 Pore size interaction plot between (a) composition, (b) holes and (c) rpm

Similarly, the deformation behavior and stress-strain graphs from the compression test for the standing position (in the XZ plane, as shown in Fig. 3) of the developed foam are illustrated in Fig. 18(a), (b), (c), (d), and (e). Figure 18(a) depicts the initial position of the sample, while Fig. 18(b), (c), and (d) show the deformation from 30 to 80% of the sample. These figures clearly demonstrate that deformation begins at the sample's contact point and extends to the machine's head, highlighted in the red circle in Fig. 18(b). In this position, the stress-strain graph indicates less force absorption capacity and a longer strain zone compared to samples in a flat position (XY

plane). To gain a clearer understanding of the compression test parameters, the effect of porosity on deformation behavior was also examined in this direction. The compression behavior of samples with 8, 10, and 12 holes is shown in Fig. 19(a), (b), and (c). These data reveal that as the number of holes in a consumable rod increases, porosity increases, thereby enhancing the sample's deformation range. The plateau zones, which can be used to calculate the foam's deformation range, are crucial for determining the developed foam's force-absorbing capacity (Ref 24).

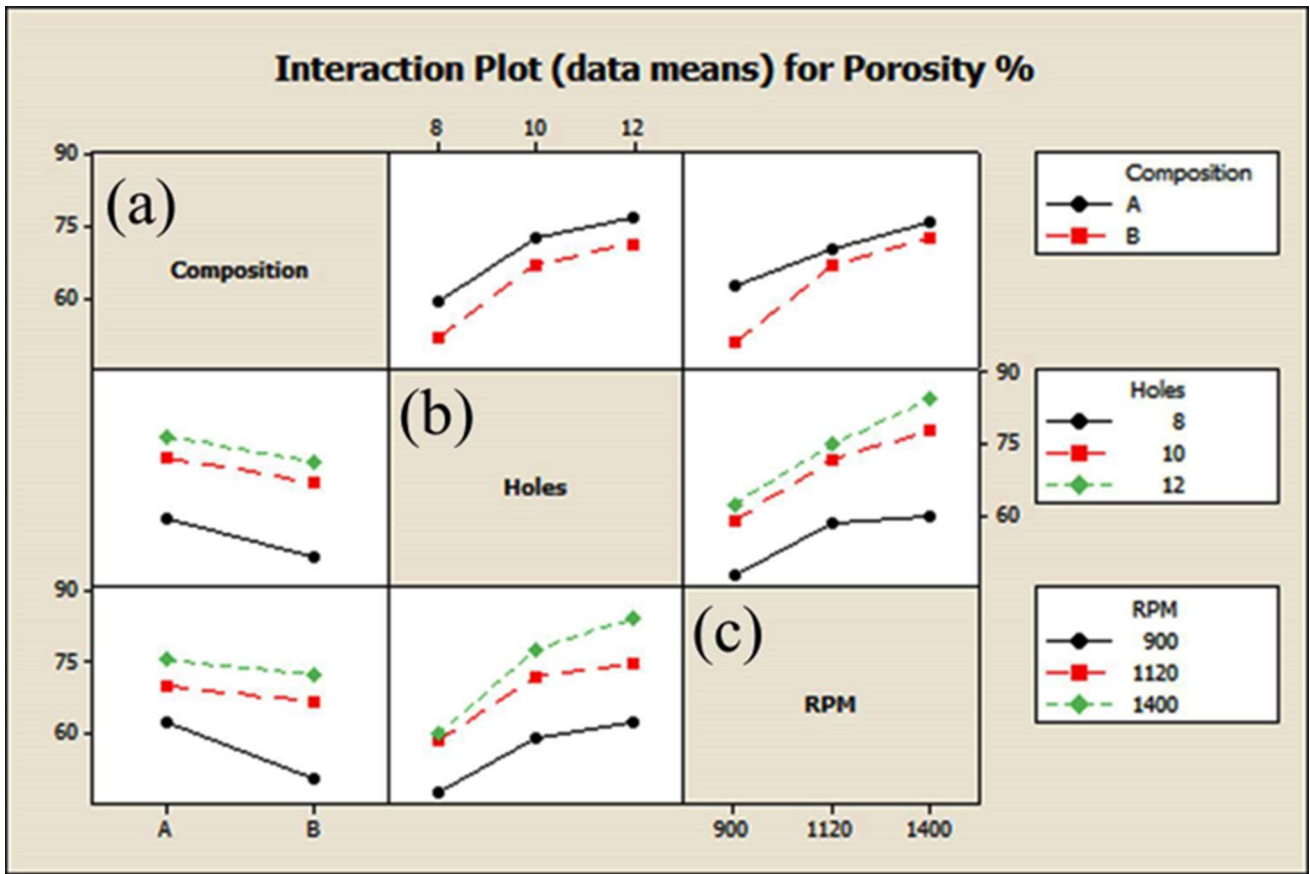


Fig. 15 Porosity % interaction plot between (a) composition, (b) holes and (c) rpm

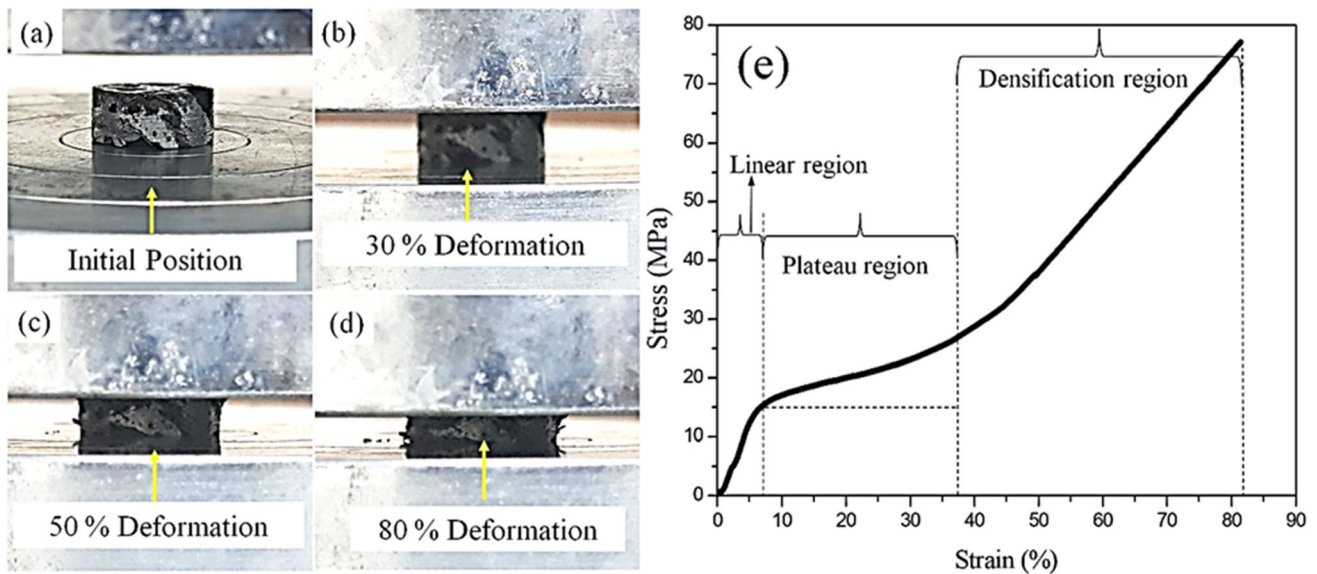


Fig. 16 Deformation of the foam in % during compression in flat position; (a) 0%, (b) 10%, (c) 50%, (d) 80% and (e) stress-strain graph

The foam developed with 12 holes demonstrates a significant plateau zone, characterized by constant material deformation. Compared to foams with 8 or 10 holes, the plateau zone is more extensive in those with 12 holes. This difference arises from the distribution, size, and thickness of the walls between

the pores, which influence the plateau zone's nature. Initially, the plateau stress increases to a peak and then declines as the number of pores increases, due to the need for an optimal wall thickness for greater deformation. This study also reveals that as wall thickness increases and the number of pores decreases,

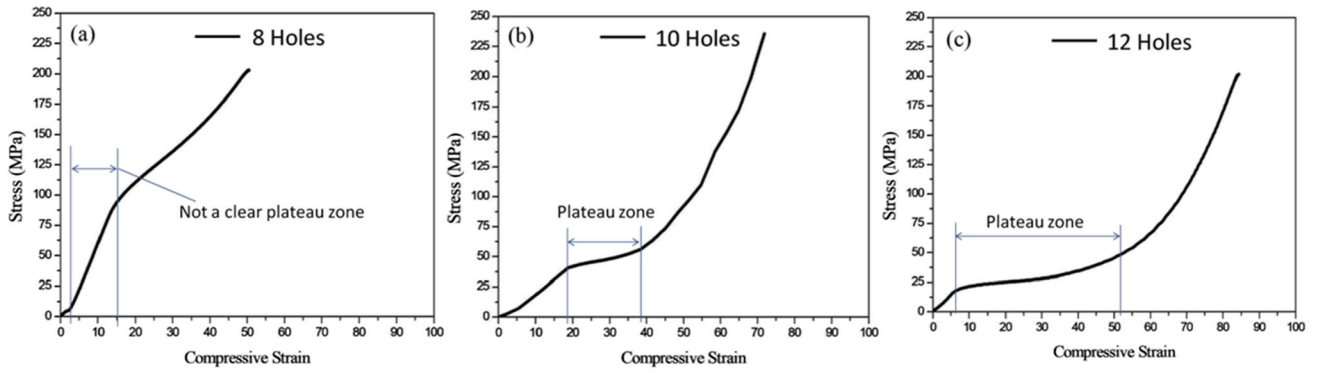


Fig. 17 The stress-strain diagram of developed sample in flat position with (a) 8 (b) 10 and (c) 12 holes with 1400 rpm and 60% titanium hydrate composition

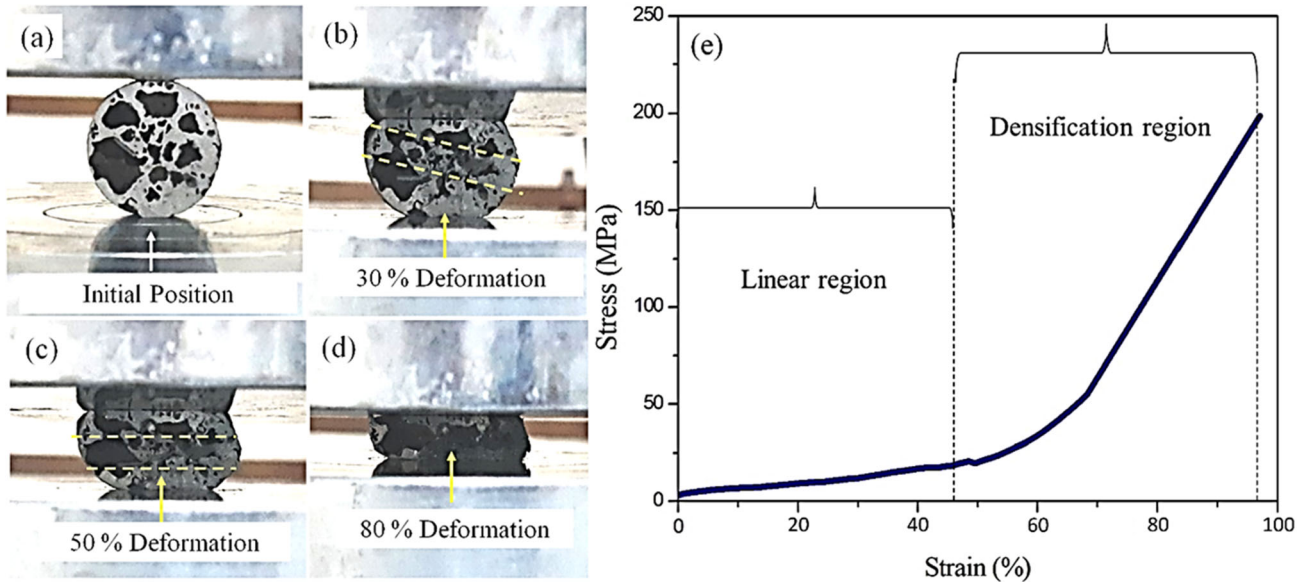


Fig. 18 Deformation of the foam in % during compression in standing position; (a) 0%, (b) 30%, (c) 50%, (d) 80% and (e) stress-strain graph

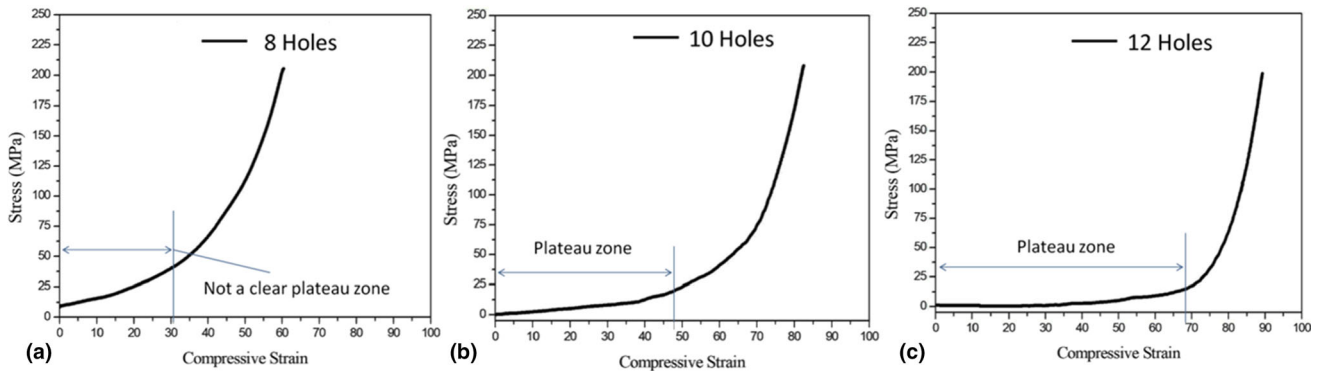


Fig. 19 The stress-strain diagram of developed sample in standing position with (a) 8, (b) 10 and (c) 12 holes with 1400 rpm and 60% titanium hydrate composition

as seen in foams with 8 holes, deformation correlates with increased stress and strain. The plateau zone remains uniform in foams with 10 and 12 holes, owing to correct pore distribution

and reduced wall thickness. Nonetheless, slight variations in the length of plateau stress and the initial deformation stage occur due to differences in pore structures among the samples.

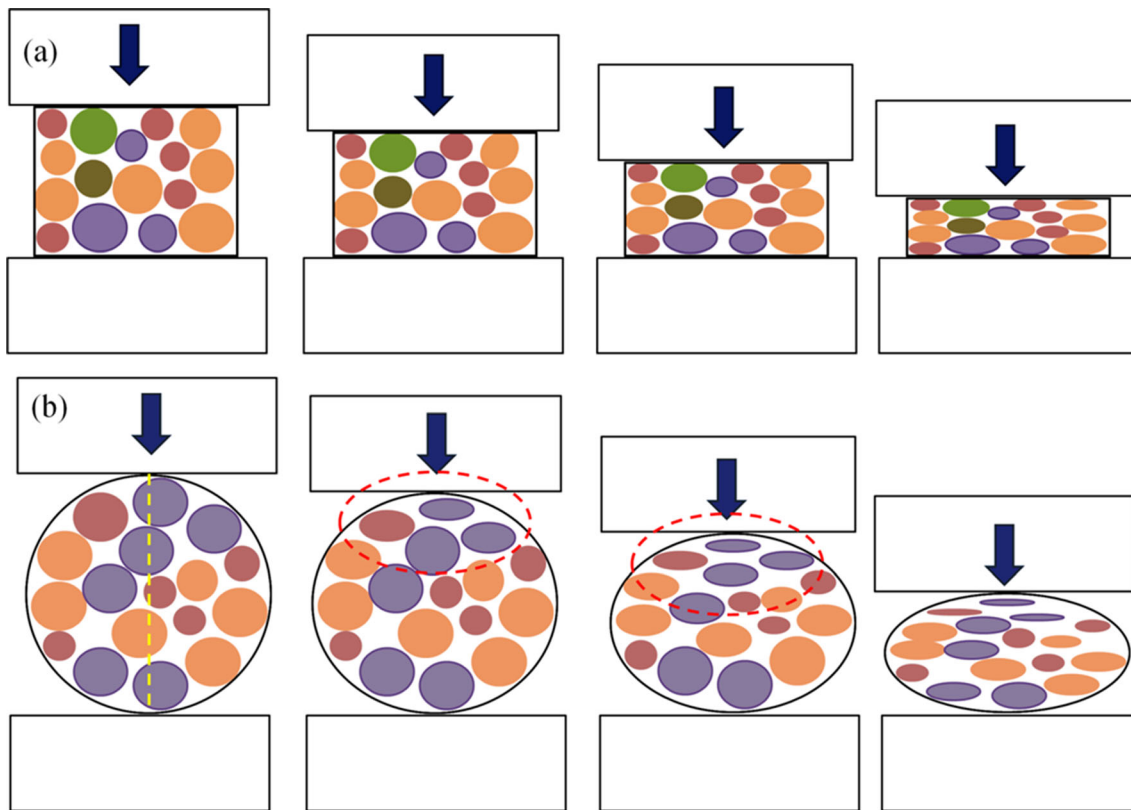


Fig. 20 Deformation mechanism of foam sample in (a) flat position and (b) in vertical position

The deformation pattern in two different orientations is different, which shows an anisotropic behavior of developed foam. This anisotropic behavior depends on the failure mechanism of the walls of the porous structure. Figure 20 shows the schematic failure mechanisms in the different orientations of developed porous samples. Figure 20(a) shows the failure mechanism in flat conditions (XY plane). In this mechanism, the deformation takes place from a large surface, and thus, the sample initially shows a sharp increase in stress in the first stage of deformation, while this increased stress is reduced in the second stage, where the walls of the foam material start deforming. However, this phenomenon is not seen in the sample in a standing position. Figure 20(b) shows the deformation mechanism in the sample in a standing position (XZ plane). The deformation in this position starts at the contact point of the moving crosshead and sample. Here, the contact is line contact, whereas, in the flat sample, the contact is area contact. Thus, due to line contact, very little force is required to deform the sample, and thus, a large strain with a very small increase in stress is observed in this position. This phenomenon is shown in Fig. 20(b) in red circle. This deformation continues until the deformation reaches a sufficient contact area between the crosshead and sample, and after that, stress increases sharply with strain.

4. Conclusions

Efficient foam is made using the friction stir tube deposition method. Initially, the deposition method is used to put the foamable precursor in the tube. Later, the precursor is heated to

create the foam. The foam produced is then studied for its mechanical properties and metallurgical characteristics. The results obtained lead to the following conclusions.

- The clustering of particles was observed in the deposited material with fewer holes and at lower rpm.
- The uniform distribution of foaming powder is obtained with 10- and 12-hole profile rods, as observed by microstructural analysis of material flow. The grain refinement is also observed with a higher value of the rotational speed of the consumable rod.
- A 60% decrease in pore size is obtained when the holes in the consumable rod increase from 8 to 12.
- The 8-hole configuration rod does not show a proper plateau zone in any orientation.
- A 55% increase in the plateau zone in the flat position is observed with an increase in holes from 10 to 12, whereas in the vertical position, this increase is only 28%.

References

1. R. Kuziak, R. Kawalla, and S. Waengler, Advanced High Strength Steels for Automotive Industry, *J. Arch. Civ. Mech. Eng.*, 2008, **8**(2), p 103–117
2. M.K. Kulekci, Magnesium and Its Alloys Applications in Automotive Industry, *Int. J. Adv. Manuf. Technol.*, 2008, **39**, p 851–865
3. F. Simancik, Introduction: The Strange World of Cellular Metals, *Handbook of Cellular Metals: Production, Processing, Applications*. Wiley, Amsterdam, 2002, p 1–4

4. L. Gibson and M. Ashby, *Cellular Solids: Structure & Properties*, Vol 9 Pergamon Press, Oxford, 1989, p 165-166.2
5. S. Rathee, S. Maheshwari, A.N. Siddiquee, and M. Srivastava, A Review of Recent Progress in Solid State Fabrication of Composites and Functionally Graded Systems Via Friction Stir Processing, *J. Crit. Rev. Solid State*, 2018, **43**(4), p 334–366
6. Q. Pang, J. Zheng, and Z.-L. Hu, Microstructural Characteristics and Mechanical Properties of 7075 Aluminum Alloy Foam Sandwich Panels Fabricated Via Integrated Forming and Foaming, *J. Manuf. Process.*, 2023, **94**, p 133–145
7. J. Banhart, Aluminium Foams for Lighter Vehicles, *Int. J. Veh. Des.*, 2005, **37**(2–3), p 114–125
8. T. Hamada, H. Kanahashi, and N. Kanetake, Axial Crushing Performance of Porous Aluminum Filled Members, *J. Japan Inst. Metals*, 2009, **73**(6), p 453–461
9. I. Duarte, L. Krstulović-Opara, and M. Vesjenjak, Characterisation of Aluminium Alloy Tubes Filled with Aluminium Alloy Integral-Skin Foam under Axial Compressive Loads, *Compos. Struct.*, 2015, **121**, p 154–162
10. I. Duarte, M. Vesjenjak, and L. Krstulović-Opara, Dynamic and Quasi-Static Bending Behaviour of Thin-Walled Aluminium Tubes Filled with Aluminium Foam, *Compos. Struct.*, 2014, **109**, p 48–56
11. A.K. Toksoy, M. Tanoğlu, M. Güden, and I.W. Hall, Effect of Adhesive on the Strengthening of Aluminum Foam-Filled Circular Tubes, *J. Mater. Sci.*, 2004, **39**, p 1503
12. M. Talebi, P. Asadi, and M. Akbari, Friction Stir Extrusion and Mechanical Alloying of LM13 Casting Ingot to Produce LM28 Tubes, *J. Mater. Res. Technol.*, 2023, **27**, p 6672–6687
13. J. Banhart and H.W. Seeliger, Aluminium Foam Sandwich Panels: Manufacture, Metallurgy And Applications, *Adv. Eng. Mater.*, 2008, **10**(9), p 793–802
14. Y. Song, L. Xiao, X. Zhao, H. Zhou, W. Zhang, L. Guo, and Y. Wang, Fabrication, Microstructure and Shear Properties of Al Foam Sandwich, *Mater. Manuf. Process.*, 2016, **31**(8), p 1046–1051
15. S. Rathee, S. Maheshwari, and A.N. Siddiquee, Issues and Strategies in Composite Fabrication via Friction Stir Processing: A Review, *Mater. Manuf. Process.*, 2018, **33**(3), p 239–261
16. S. Bharti, N.D. Ghetiya, and K.M. Patel, A Review on Manufacturing the Surface Composites by Friction Stir Processing, *Mater. Manuf. Process.*, 2021, **36**(2), p 135–170
17. P. Asadi and M. Akbari, Numerical Modeling and Experimental Investigation of Brass Wire Forming by Friction Stir Back Extrusion, *Int. J. Adv. Manuf. Technol.*, 2021, **116**, p 3231–3245
18. Y. Hangai, K. Takada, R. Endoh, S. Koyama, and T. Utsunomiya, Foaming Behavior of Aluminum Foam Precursor Induced by Friction Heat Generated by Rotating Tool Used for Spot Friction Stir Welding, *J. Manuf. Process.*, 2017, **25**, p 426–431
19. M. Akbari and P. Asadi, Optimization of Microstructural and Mechanical Properties of Brass Wire Produced by Friction Stir Extrusion Using Taguchi Method, *Proc. Inst. Mech. Eng. Part L J. Mater. Des. Appl.*, 2021, **235**(12), p 2709–2719
20. H. Dong, X. Li, K. Xu, Z. Zang, X. Liu, Z. Zhang, W. Xiao, and Y. Li, A review on solid-state-based additive friction stir deposition, *Aero-space*, 2022, **9**(10), p 565
21. F. Khodabakhshi and A.J. Gerlich, Potentials and Strategies of Solid-State Additive Friction-Stir Manufacturing Technology: A Critical Review, *J. Manuf. Process.*, 2018, **36**, p 77–92
22. M.S. Khorrami and M. Movahedi, Microstructure Evolutions and Mechanical Properties of Tubular Aluminum Produced by Friction Stir Back Extrusion, *Mater. Des.*, 2015, **65**, p 74–79
23. M. Kumar, R.K.R. Singh, and V. Jain, Characterization of Mechanical and Metallurgical Properties of AA6063 Foam Developed by Friction Stir Precursor Deposition Technique, *J. Adhes. Sci. Technol.*, 2022, **37**, p 1–18
24. M. Kumar, R.K.R. Singh, and V. Jain, Effect of Tool Pin Profiles on the Properties of Foamable Precursor Developed by Friction Stir Processing, *Proc. Inst. Mech. Eng. Part E J. Process Mech. Eng.*, 2022, **237**, p 1367. <https://doi.org/10.1177/09544089221113562>
25. L.J. Gibson and M.F. Ashby, *Cellular Solids: Structure and Properties*, 2nd ed. The Press Syndicate of the University of Cambridge, Cambridge, 1997
26. M. Kumar, R.K. Raj Singh, and V. Jain, Effect of Processing Parameters and Heat Treatment Techniques on Foaming Properties of Aluminium Foam Developed by Friction Stir Processing Route, *Proc. Inst. Mech. Eng. Part L J. Mater. Des. Appl.*, 2022, **237**, p 387. <https://doi.org/10.1177/14644207221117517>

Publisher's Note Springer Nature remains neutral with regard to jurisdictional claims in published maps and institutional affiliations.

Springer Nature or its licensor (e.g. a society or other partner) holds exclusive rights to this article under a publishing agreement with the author(s) or other rightsholder(s); author self-archiving of the accepted manuscript version of this article is solely governed by the terms of such publishing agreement and applicable law.